EARTHQUAKE ENGINEERING AND STRUCTURAL DYNAMICS
*Earthquake Engng Struct. Dyn.* 2009; **38**:377–401
Published online 19 November 2008 in Wiley InterScience (www.interscience.wiley.com). DOI: 10.1002/eqe.862

# Decentralized $\mathscr{H}_\infty$ controller design for large-scale civil structures

Yang Wang[1,*,†], Jerome P. Lynch[2] and Kincho H. Law[3]

[1]*School of Civil and Environmental Engineering, Georgia Institute of Technology, Atlanta, GA 30332, U.S.A.*
[2]*Department of Civil and Environmental Engineering, University of Michigan, Ann Arbor, MI 48109, U.S.A.*
[3]*Department of Civil and Environmental Engineering, Stanford University, Stanford, CA 94305, U.S.A.*

SUMMARY

Complexities inherent to large-scale modern civil structures pose many challenges in the design of feedback structural control systems for dynamic response mitigation. With the emergence of low-cost sensors and control devices creating technologies from which large-scale structural control systems can deploy, a future control system may contain hundreds, or even thousands, of such devices. Key issues in such large-scale structural control systems include reduced system reliability, increasing communication requirements, and longer latencies in the feedback loop. To effectively address these issues, decentralized control strategies provide promising solutions that allow control systems to operate at high nodal counts.

This paper examines the feasibility of designing a decentralized controller that minimizes the $\mathscr{H}_\infty$ norm of the closed-loop system. $\mathscr{H}_\infty$ control is a natural choice for decentralization because imposition of decentralized architectures is easy to achieve when posing the controller design using linear matrix inequalities. Decentralized control solutions are investigated for both continuous-time and discrete-time $\mathscr{H}_\infty$ formulations. Numerical simulation results using a 3-story and a 20-story structure illustrate the feasibility of the different decentralized control strategies. The results also demonstrate that when realistic semi-active control devices are used in combination with the decentralized $\mathscr{H}_\infty$ control solution, better performance can be gained over the passive control cases. It is shown that decentralized control strategies may provide equivalent or better control performance, given that their centralized counterparts could suffer from longer sampling periods due to communication and computation constraints. Copyright © 2008 John Wiley & Sons, Ltd.

Received 19 June 2008; Revised 8 September 2008; Accepted 9 September 2008

KEY WORDS: H-infinity control; feedback structural control; decentralized control; smart structures

*Correspondence to: Yang Wang, School of Civil and Environmental Engineering, Georgia Institute of Technology, Atlanta, GA 30332, U.S.A.
†E-mail: yang.wang@ce.gatech.edu

Contract/grant sponsor: Office of Naval Research
Contract/grant sponsor: Office of Technology Licensing Stanford Graduate Fellowship
Contract/grant sponsor: NSF; contract/grant number: CMMI-0824977

## 1. INTRODUCTION

Real-time feedback control has been a topic of great interest to the structural engineering community over the last few decades [1–4]. A feedback structural control system includes an integrated network of sensors, controllers, and control devices that are installed in the civil structure to mitigate undesired vibrations during external excitations, such as earthquakes or typhoons. Under an external excitation, the dynamic response of the structure is measured by sensors. Sensor data are communicated to a centralized controller that uses the data to calculate an optimal control solution. The optimal solution is then dispatched by the controller to control devices, which directly (i.e. active devices) or indirectly (i.e. semi-active devices) apply forces to the structure. This process repeats continuously in real time to mitigate, or even eliminate, undesired structural vibrations. It was recently reported that more than 50 buildings and towers have been successfully instrumented with various types of structural control systems from 1989 to 2003 [5]. In practice, semi-active control is usually preferred over active control because it can achieve at least an equivalent level of performance, consumes orders of magnitude less power, and provides higher level of reliability. Examples of semi-active control devices include active variable stiffness devices, semi-active hydraulic dampers (SHD), electrorheological dampers, and magnetorheological dampers [6]. Additional advantages associated with semi-active control include adaptability to real-time excitation, inherent bounded input/bounded output stability, and invulnerability against power failure.

Traditional feedback structural control systems employ centralized architectures. In such an architecture, one central controller is responsible for collecting data from all the sensors in the structure, making control decisions, and dispatching these control decisions to control devices. Hence, the requirements on communication range and data transmission bandwidth increase with the size of the structure and with the number of sensors and control devices being deployed. The communication requirements could impose economical and technical difficulties for the implementation of feedback control systems in increasingly larger civil structures. The centralized controller itself represents a single point of potential failure; failure of the controller may paralyze the entire control system. In order to overcome these inherent challenges, decentralized control architectures could be alternatively adopted [7–9]. For example, a structural control system consisting of 88 fully decentralized semi-active oil dampers has been installed in the 170 m-tall Shiodome Tower in Tokyo, Japan [10, 11].

This paper examines both fully decentralized scheme, where the controller on a floor only has local sensor data from that floor, and partially decentralized scheme, where the controller also receives sensor data from neighboring floors (or substructures). In a decentralized control system architecture, multiple controllers are distributed throughout the structure. Acquiring data from a local subnet of sensors, each controller commands control devices in its vicinity. The benefits of localizing a subset of sensors and control devices to each controller include shorter communication ranges and reduced data transmission rates in the control system. Decentralization also eliminates the risk of global control system failure if one of the controllers should fail. For large-scale structures, occasional failure of decentralized controllers may only cause minor degradation to the control performance.

Decentralized control design based on the linear quadratic regulator (LQR) optimization criteria has been previously explored by the authors to study the feasibility of utilizing wireless sensors as controllers for feedback structural control [12, 13]. This paper investigates a different approach to the design of a decentralized control system based on $\mathscr{H}_\infty$ control theory, which is known to offer excellent control performance when 'worst-case' external disturbances are encountered. Owing to



DOI: 10.1002/eqe

the multiplicative property of the $\mathscr{H}_\infty$ norm [14], $\mathscr{H}_\infty$ control design can also consider modeling uncertainties (as is typical in most civil structures). Centralized $\mathscr{H}_\infty$ controller implementation in the continuous-time domain for civil structural control has been extensively studied [15–21]. When compared with traditional linear quadratic Gaussian controllers, $\mathscr{H}_\infty$ controllers can achieve either comparable or superior performance [22, 23]. For example, it has been shown that $\mathscr{H}_\infty$ control design may achieve better performance in attenuating transient vibrations of the structure [24]. However, decentralized $\mathscr{H}_\infty$ controller design, either in the continuous-time domain or discrete-time domain, has rarely been explored in structural control.

The $\mathscr{H}_\infty$ control solution can be readily formulated as an optimization problem with constraints expressed in terms of linear matrix inequalities (LMI) [25]. For such problems, sparsity patterns can be easily applied to the controller matrix variables. This property offers significant convenience for designing decentralized controllers, where certain sparsity patterns can be applied to the gain matrices consistent with certain desired feedback architecture. This paper presents pilot studies investigating the feasibility of decentralized $\mathscr{H}_\infty$ control that may be employed in large-scale structural control systems. More specifically, decentralized $\mathscr{H}_\infty$ controller design is presented in both the continuous-time and discrete-time domains. Using properties of LMI, the decentralized $\mathscr{H}_\infty$ control problem is converted into a convex optimization problem that can be conveniently solved using available mathematical packages.

Numerical simulations are conducted to validate the performance of the decentralized $\mathscr{H}_\infty$ controller design. In the first example, a 3-story structure is used to demonstrate the detailed procedure for the design of the decentralized $\mathscr{H}_\infty$ controller. The control performance of decentralized $\mathscr{H}_\infty$ controllers is then compared with the performance of decentralized LQR-based controllers [12, 13]. In the second example, simulations of a 20-story benchmark structure are conducted to illustrate the efficacy of the decentralized $\mathscr{H}_\infty$ control solution for large-scale civil structures. Different information feedback architectures and control sampling rates are employed so as to provide an in-depth study of the proposed approaches. Control performance using ideal actuators and large-capacity SHD dampers are presented for the 20-story structure. Performance of the decentralized control system is compared with passive control cases where the SHD dampers are fixed at minimum or maximum damping settings.

## 2. FORMULATION OF DECENTRALIZED $\mathscr{H}_\infty$ CONTROL

This section first discusses the design of a decentralized $\mathscr{H}_\infty$ controller for structural control in the continuous-time domain. The controller's counterpart in the discrete-time domain is then derived. In both derivations, properties of LMI are utilized to convert the formulation of the decentralized control design problem into a convex optimization problem.

### *2.1. Continuous-time decentralized $\mathscr{H}_\infty$ control*

For a lumped-mass structural model with $n$ degrees-of-freedom subjected to $m_1$ external excitations, and controlled by $m_2$ control devices, the equations of motion can be formulated as

$$\mathbf{M}\ddot{\mathbf{q}}(t)+\mathbf{C}\dot{\mathbf{q}}(t)+\mathbf{K}\mathbf{q}(t)=\mathbf{T}_\mathbf{u}\mathbf{u}(t)+\mathbf{T}_\mathbf{w}\mathbf{w}(t) \tag{1}$$

where $\mathbf{q}(t)\in\mathbb{R}^{n\times 1}$ is the displacement vector relative to the ground; $\mathbf{M}$, $\mathbf{C}$, $\mathbf{K}\in\mathbb{R}^{n\times n}$ are the mass, damping, and stiffness matrices, respectively; $\mathbf{u}(t)\in\mathbb{R}^{m_2\times 1}$ and $\mathbf{w}(t)\in\mathbb{R}^{m_1\times 1}$ are the control force



DOI: 10.1002/eqe

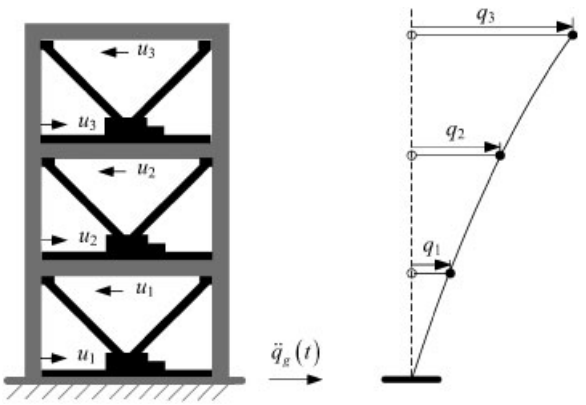


Figure 1. A three-story controlled structure excited by unidirectional ground motion.

and external excitation vectors, respectively; and $\mathbf{T_u} \in \mathbb{R}^{n \times m_2}$ and $\mathbf{T_w} \in \mathbb{R}^{n \times m_1}$ are the control and excitation location matrices, respectively.

For simplicity, the discussion is based on a 2D shear–frame structure subjected to unidirectional ground excitation. In the example structure shown in Figure 1, it is assumed that the external excitation, $\mathbf{w}(t)$, is a scalar function ($m_1 = 1$) containing the ground acceleration time history $\ddot{q}_g(t)$; the spatial load pattern $\mathbf{T_w}$ is then equal to $-\mathbf{M}\{\mathbf{1}\}_{n\times 1}$. Entries in $\mathbf{u}(t)$ are defined as the control forces between neighboring floors. For the 3-story structure, if a positive control force is defined to be moving the floor above the device toward the left direction, and moving the floor below the device toward the right direction (as shown in Figure 1), the control force location matrix $\mathbf{T_u}$ is defined as

$$\mathbf{T_u} = \begin{bmatrix} -1 & 1 & 0 \\ 0 & -1 & 1 \\ 0 & 0 & -1 \end{bmatrix} \tag{2}$$

The second-order ordinary differential equation (ODE), Equation (1), can be converted to a first-order ODE by the state-space formulation as follows:

$$\dot{\mathbf{x}}_\mathbf{I}(t) = \mathbf{A_I}\mathbf{x_I}(t) + \mathbf{B_I}\mathbf{u}(t) + \mathbf{E_I}\mathbf{w}(t) \tag{3}$$

where $\mathbf{x_I} = [\mathbf{q}(t); \dot{\mathbf{q}}(t)] \in \mathbb{R}^{2n\times 1}$ is the state vector; $\mathbf{A_I} \in \mathbb{R}^{2n\times 2n}$, $\mathbf{B_I} \in \mathbb{R}^{2n\times m_2}$, and $\mathbf{E_I} \in \mathbb{R}^{2n\times m_1}$ are the system, control, and excitation matrices, respectively:

$$\mathbf{A_I} = \begin{bmatrix} [\mathbf{0}]_{n\times n} & [\mathbf{I}]_{n\times n} \\ -\mathbf{M^{-1}K} & -\mathbf{M^{-1}C} \end{bmatrix}, \quad \mathbf{B_I} = \begin{bmatrix} [\mathbf{0}]_{n\times m_2} \\ \mathbf{M^{-1}T_u} \end{bmatrix}, \quad \mathbf{E_I} = \begin{bmatrix} \{\mathbf{0}\}_{n\times 1} \\ -\{\mathbf{1}\}_{n\times 1} \end{bmatrix} \tag{4}$$

In this study, it is assumed that inter-story drifts and velocities are measurable. The displacement and velocity variables in $\mathbf{x_I}$, which are relative to the ground, are first transformed into inter-story drifts and velocities (i.e. drifts and velocities between neighboring floors). The inter-story drifts and velocities at each story are then grouped together as:

$$\mathbf{x} = [q_1 \;\; \dot{q}_1 \;\; q_2 \;\; -q_1 \;\; \dot{q}_2 - \dot{q}_1, \ldots, q_n - q_{n-1} \;\; \dot{q}_n - \dot{q}_{n-1}]^\mathrm{T} \tag{5}$$



DOI: 10.1002/eqe

A linear transformation matrix $\mathbf{\Gamma} \in \mathbb{R}^{2n \times 2n}$ can be defined such that $\mathbf{x} = \mathbf{\Gamma}\mathbf{x}_\mathrm{I}$. Substituting $\mathbf{x}_\mathrm{I} = \mathbf{\Gamma}^{-1}\mathbf{x}$ into Equation (3), and left multiplying the equation with $\mathbf{\Gamma}$, the state-space representation with the transformed (inter-story) state vector becomes

$$\dot{\mathbf{x}}(t) = \mathbf{A}\mathbf{x}(t) + \mathbf{B}\mathbf{u}(t) + \mathbf{E}\mathbf{w}(t) \tag{6}$$

where

$$\mathbf{A} = \mathbf{\Gamma}\mathbf{A}_\mathrm{I}\mathbf{\Gamma}^{-1}, \quad \mathbf{B} = \mathbf{\Gamma}\mathbf{B}_\mathrm{I}, \quad \mathbf{E} = \mathbf{\Gamma}\mathbf{E}_\mathrm{I} \tag{7}$$

The system output $\mathbf{z}(t) \in \mathbb{R}^{p \times 1}$ is defined as the sum of linear transformations to the state vector $\mathbf{x}(t)$ and the control force vector $\mathbf{u}(t)$:

$$\mathbf{z}(t) = \mathbf{C}_\mathbf{z}\mathbf{x}(t) + \mathbf{D}_\mathbf{z}\mathbf{u}(t) \tag{8}$$

where $\mathbf{C}_\mathbf{z} \in \mathbb{R}^{p \times 2n}$ and $\mathbf{D}_\mathbf{z} \in \mathbb{R}^{p \times m_2}$ are the output matrices for the state and control force vectors, respectively. Assuming static state feedback, the control force $\mathbf{u}(t)$ is determined by $\mathbf{u}(t) = \mathbf{G}\mathbf{x}(t)$, where $\mathbf{G} \in \mathbb{R}^{m_2 \times 2n}$ is termed the control gain matrix. Substituting $\mathbf{G}\mathbf{x}(t)$ for $\mathbf{u}(t)$ in Equations (6) and (8), the state-space equations of the closed-loop system can be written as:

$$\begin{aligned} \dot{\mathbf{x}}(t) &= \mathbf{A}_\mathrm{CL}\mathbf{x}(t) + \mathbf{E}\mathbf{w}(t) \\ \mathbf{z}(t) &= \mathbf{C}_\mathrm{CL}\mathbf{x}(t) \end{aligned} \tag{9}$$

where

$$\begin{aligned} \mathbf{A}_\mathrm{CL} &= \mathbf{A} + \mathbf{B}\mathbf{G} \\ \mathbf{C}_\mathrm{CL} &= \mathbf{C}_\mathbf{z} + \mathbf{D}_\mathbf{z}\mathbf{G} \end{aligned} \tag{10}$$

In frequency domain, the system dynamics can be represented by the transfer function $\mathbf{H}_\mathbf{zw}(s) \in \mathbb{C}^{p \times m_1}$ from disturbance $\mathbf{w}(t)$ to output $\mathbf{z}(t)$ as [26]

$$\mathbf{H}_\mathbf{zw}(s) = \mathbf{C}_\mathrm{CL}(s\mathbf{I} - \mathbf{A}_\mathrm{CL})^{-1}\mathbf{E} \tag{11}$$

where $s$ is the complex Laplacian variable. The objective of $\mathscr{H}_\infty$ control is to minimize the $\mathscr{H}_\infty$-norm of the closed-loop system, which in the frequency domain is defined as

$$\|\mathbf{H}_\mathbf{zw}(s)\|_\infty = \sup_\omega \bar{\sigma}[\mathbf{H}_\mathbf{zw}(j\omega)] \tag{12}$$

where $\omega$ represents angular frequency, $j$ is the imaginary unit, $\bar{\sigma}[\cdot]$ denotes the largest singular value of a matrix, and 'sup' denotes the supremum (least upper bound) of a set of real numbers. The definition shows that in the frequency domain, the $\mathscr{H}_\infty$-norm of the system is equal to the peak of the largest singular value of the transfer function $\mathbf{H}_\mathbf{zw}(s)$ along the imaginary axis (where $s = j\omega$). The $\mathscr{H}_\infty$-norm also has an equivalent interpretation in the time domain, as the supremum of the 2-norm amplification from the disturbance to the output:

$$\|\mathbf{H}_\mathbf{zw}(s)\|_\infty = \sup_{\mathbf{w}, \|\mathbf{w}(t)\|_2 \neq 0} (\|\mathbf{z}(t)\|_2 / \|\mathbf{w}(t)\|_2) \tag{13}$$

where the 2-norm of a signal $\mathbf{f}(t)$ is defined as $\|\mathbf{f}(t)\|_2 = \sqrt{\int_{t=-\infty}^{t=+\infty} \mathbf{f}^\mathrm{T}(t)\mathbf{f}(t)\,\mathrm{d}t}$, which represents the energy level of a signal. In this study, the $\mathscr{H}_\infty$-norm can be viewed as the upper limit of



DOI: 10.1002/eqe

the amplification factor from the disturbance (i.e. seismic ground motion) energy to the output (i.e. structural response) energy. The disturbance is called a 'worst-case' disturbance when this upper limit is reached. By minimizing the $\mathscr{H}_\infty$-norm, the system output (which includes structural response measures) can be greatly reduced when a worst-case disturbance (which is the earthquake excitation) is applied.

According to the Bounded Real Lemma, the following two statements are equivalent for a $\mathscr{H}_\infty$ controller that minimizes the smallest upper bound of the $\mathscr{H}_\infty$-norm of a continuous-time system [25]:

1. $\|\mathbf{H_{zw}}\|_\infty < \gamma$ and $\mathbf{A}_{\mathrm{CL}}$ is stable in the continuous-time sense (i.e. the real parts of all the eigenvalues of $\mathbf{A}_{\mathrm{CL}}$ are negative).
2. There exists a symmetric positive-definite matrix $\mathbf{\Theta} \in \mathbb{R}^{2n\times 2n}$ such that the following inequality holds:

$$\begin{bmatrix} \mathbf{A}_{\mathrm{CL}}\mathbf{\Theta} + \mathbf{\Theta}\mathbf{A}_{\mathrm{CL}}^{\mathrm{T}} + \mathbf{E}\mathbf{E}^{\mathrm{T}}/\gamma^2 & \mathbf{\Theta}\mathbf{C}_{\mathrm{CL}}^{\mathrm{T}} \\ * & -\mathbf{I} \end{bmatrix} < 0 \tag{14}$$

where $*$ denotes the symmetric entry (in this case, $\mathbf{C}_{\mathrm{CL}}\mathbf{\Theta}$), and '$<0$' means that the matrix at the left side of the inequality is negative definite. Using the closed-loop matrix definitions in Equation (10), Equation (14) becomes

$$\begin{bmatrix} \mathbf{A}\mathbf{\Theta} + \mathbf{\Theta}\mathbf{A}^{\mathrm{T}} + \mathbf{B}\mathbf{G}\mathbf{\Theta} + \mathbf{\Theta}\mathbf{G}^{\mathrm{T}}\mathbf{B}^{\mathrm{T}} + \mathbf{E}\mathbf{E}^{\mathrm{T}}/\gamma^2 & \mathbf{\Theta}\mathbf{C}_{\mathbf{z}}^{\mathrm{T}} + \mathbf{\Theta}\mathbf{G}^{\mathrm{T}}\mathbf{D}_{\mathbf{z}}^{\mathrm{T}} \\ * & -\mathbf{I} \end{bmatrix} < 0 \tag{15}$$

The above nonlinear matrix inequality can be converted into LMI by introducing a new variable $\mathbf{Y} \in \mathbb{R}^{m_2\times 2n}$ where $\mathbf{Y} = \mathbf{G}\mathbf{\Theta}$

$$\begin{bmatrix} \mathbf{A}\mathbf{\Theta} + \mathbf{\Theta}\mathbf{A}^{\mathrm{T}} + \mathbf{B}\mathbf{Y} + \mathbf{Y}^{\mathrm{T}}\mathbf{B}^{\mathrm{T}} + \mathbf{E}\mathbf{E}^{\mathrm{T}}/\gamma^2 & \mathbf{\Theta}\mathbf{C}_{\mathbf{z}}^{\mathrm{T}} + \mathbf{Y}^{\mathrm{T}}\mathbf{D}_{\mathbf{z}}^{\mathrm{T}} \\ * & -\mathbf{I} \end{bmatrix} < 0 \tag{16}$$

In summary, the continuous-time $\mathscr{H}_\infty$ control problem is now transformed into a convex optimization problem:

$$\begin{aligned} &\text{minimize} && \gamma \\ &\text{subject to} && \mathbf{\Theta} > 0 \text{ and the LMI expressed in Equation (16)} \end{aligned} \tag{17}$$

Here $\mathbf{Y}$, $\mathbf{\Theta}$, and $\gamma$ are the optimization variables. Numerical solutions to this optimization problem can be computed, for example, using the Matlab LMI Toolbox [27] or the convex optimization package CVX [28]. After the optimization problem is solved, the control gain matrix is computed as:

$$\mathbf{G} = \mathbf{Y}\mathbf{\Theta}^{-1} \tag{18}$$

In general, the algorithm finds a gain matrix without any sparsity constraints; in other words, it represents a control scheme consistent with a centralized state feedback architecture. To compute gain matrices for decentralized state feedback control, appropriate sparsity constraints can be applied to the optimization variables $\mathbf{Y}$ and $\mathbf{\Theta}$ while solving the optimization problem of



DOI: 10.1002/eqe

Equation (17). For most available software packages, the sparsity constraints can be conveniently defined by assigning corresponding zero entries to the $\mathbf{Y}$ and $\mathbf{\Theta}$ optimization variables. For example, gain matrices of the following sparsity patterns may be employed for a three-story structure:

$$\mathbf{G}_{\mathrm{I}} = \begin{bmatrix} \blacksquare & 0 & 0 \\ 0 & \blacksquare & 0 \\ 0 & 0 & \blacksquare \end{bmatrix} \quad \text{and} \quad \mathbf{G}_{\mathrm{II}} = \begin{bmatrix} \blacksquare & \blacksquare & 0 \\ \blacksquare & \blacksquare & \blacksquare \\ 0 & \blacksquare & \blacksquare \end{bmatrix} \tag{19}$$

Note that each entry in the above matrices represents a $1 \times 2$ block. According to the linear feedback control law $\mathbf{u}(t) = \mathbf{G}\mathbf{x}(t)$, when the sparsity pattern in $\mathbf{G}_{\mathrm{I}}$ is used, only the inter-story drift and velocity at the $i$th story are needed to determine the control force $u_i$ at the same story. When the sparsity pattern in $\mathbf{G}_{\mathrm{II}}$ is adopted, the inter-story drifts and velocities from both the $i$th story and the neighboring stories (story) are needed in order to determine the control force $u_i$ at the $i$th story. Considering the relationship between $\mathbf{G}$ and $\mathbf{Y}$ as specified in Equation (18), in order to find the control gain matrices satisfying the shape constraints in $\mathbf{G}_{\mathrm{I}}$, the following shape constraints may be applied to the optimization variables $\mathbf{Y}$ and $\mathbf{\Theta}$:

$$\mathbf{Y}_{\mathrm{I}} = \begin{bmatrix} \blacksquare & 0 & 0 \\ 0 & \blacksquare & 0 \\ 0 & 0 & \blacksquare \end{bmatrix} \quad \text{and} \quad \mathbf{\Theta}_{\mathrm{I}} = \begin{bmatrix} \blacksquare & 0 & 0 \\ 0 & \blacksquare & 0 \\ 0 & 0 & \blacksquare \end{bmatrix} \tag{20}$$

Similarly, to compute control gain matrices satisfying the shape constraints of $\mathbf{G}_{\mathrm{II}}$, the following shape constraints may be applied to the optimization variables:

$$\mathbf{Y}_{\mathrm{II}} = \begin{bmatrix} \blacksquare & \blacksquare & 0 \\ \blacksquare & \blacksquare & \blacksquare \\ 0 & \blacksquare & \blacksquare \end{bmatrix} \quad \text{and} \quad \mathbf{\Theta}_{\mathrm{II}} = \begin{bmatrix} \blacksquare & 0 & 0 \\ 0 & \blacksquare & 0 \\ 0 & 0 & \blacksquare \end{bmatrix} \tag{21}$$

It is important to realize that due to the constraints imposed on the $\mathbf{Y}$ and $\mathbf{\Theta}$ variables, the presented decentralized $\mathscr{H}_\infty$ controller precludes the possibility that a decentralized gain matrix may exist with $\mathbf{Y}$ and $\mathbf{\Theta}$ variables not satisfying the corresponding shape constraints. For example, it is possible that a gain matrix may satisfy the sparsity pattern in $\mathbf{G}_{\mathrm{I}}$ while the corresponding $\mathbf{Y}$ and $\mathbf{\Theta}$ variables do not conform to the sparsity patterns shown in Equation (20). The application of sparsity patterns to $\mathbf{Y}$ and $\mathbf{\Theta}$ variables makes the gain matrix easily computable using existing software packages, although the approach may not be able to explore the complete solution space of decentralized gain matrices. That is, the approach for decentralized $\mathscr{H}_\infty$ controller design may not guarantee that a minimum $\mathscr{H}_\infty$-norm is obtained over the complete solution space; rather, only a minimum $\mathscr{H}_\infty$-norm is obtained for the solution space contained within the boundary imposed by the shape constraints on $\mathbf{Y}$ and $\mathbf{\Theta}$.



DOI: 10.1002/eqe

### 2.2. *Discrete-time decentralized $\mathscr{H}_\infty$ control*

For implementation in typical digital control systems, the decentralized $\mathscr{H}_\infty$ control design in discrete-time domain is needed. Using zero-order hold equivalents, the continuous-time system in Equation (9) can be transformed into an equivalent discrete-time system [29]

$$\begin{aligned} \mathbf{x}_\mathrm{d}[k+1] &= \mathbf{A}_\mathrm{dCL}\mathbf{x}_\mathrm{d}[k]+\mathbf{E}_\mathrm{d}\mathbf{w}_\mathrm{d}[k] \\ \mathbf{z}_\mathrm{d}[k] &= \mathbf{C}_\mathrm{dCL}\mathbf{x}_\mathrm{d}[k] \end{aligned} \tag{22}$$

where the subscript 'd' indicates that the variables are expressed in the discrete-time domain, and the closed-loop system matrices $\mathbf{A}_\mathrm{dCL}$ and $\mathbf{C}_\mathrm{dCL}$ are defined accordingly

$$\begin{aligned} \mathbf{A}_\mathrm{dCL} &= \mathbf{A}_\mathrm{d}+\mathbf{B}_\mathrm{d}\mathbf{G}_\mathrm{d} \\ \mathbf{C}_\mathrm{dCL} &= \mathbf{C}_\mathbf{z}+\mathbf{D}_\mathbf{z}\mathbf{G}_\mathrm{d} \end{aligned} \tag{23}$$

For linear state feedback, the control force $\mathbf{u}_\mathrm{d}[k]$ is determined as $\mathbf{u}_\mathrm{d}[k]=\mathbf{G}_\mathrm{d}\mathbf{x}_\mathrm{d}[k]$. According to the Bounded Real Lemma, the following two statements are equivalent for discrete-time systems [26]:

1. The $\mathscr{H}_\infty$-norm of the closed-loop system in Equation (22) is less than $\gamma$, and $\mathbf{A}_\mathrm{dCL}$ is stable in the discrete-time sense (i.e. all of the eigenvalues of $\mathbf{A}_\mathrm{dCL}$ fall in the unit circle on the complex plane).
2. There exists a symmetric matrix $\bar{\mathbf{\Theta}}_\mathrm{d}>0$ such that the following inequality holds:

$$\begin{bmatrix} \mathbf{A}_\mathrm{dCL}^\mathrm{T} & \mathbf{C}_\mathrm{dCL}^\mathrm{T}/\gamma \\ \mathbf{E}_\mathrm{d}^\mathrm{T} & \mathbf{0} \end{bmatrix} \begin{bmatrix} \bar{\mathbf{\Theta}}_\mathrm{d} & \mathbf{0} \\ \mathbf{0} & \mathbf{I} \end{bmatrix} \begin{bmatrix} \mathbf{A}_\mathrm{dCL} & \mathbf{E}_\mathrm{d} \\ \mathbf{C}_\mathrm{dCL}/\gamma & \mathbf{0} \end{bmatrix} - \begin{bmatrix} \bar{\mathbf{\Theta}}_\mathrm{d} & \mathbf{0} \\ \mathbf{0} & \mathbf{I} \end{bmatrix} < 0 \tag{24}$$

Replacing $\bar{\mathbf{\Theta}}_\mathrm{d}$ with $\tilde{\mathbf{\Theta}}_\mathrm{d}/\gamma^2$ and using the Schur complement [25] and congruence transformation, it can be shown that the matrix inequality in Equation (24) is equivalent to:

$$\begin{bmatrix} \tilde{\mathbf{\Theta}}_\mathrm{d} & \mathbf{0} & \mathbf{A}_\mathrm{dCL}^\mathrm{T}\tilde{\mathbf{\Theta}}_\mathrm{d} & \mathbf{C}_\mathrm{dCL}^\mathrm{T} \\ * & \gamma^2\mathbf{I} & \mathbf{E}_\mathrm{d}^\mathrm{T}\tilde{\mathbf{\Theta}}_\mathrm{d} & \mathbf{0} \\ * & * & \tilde{\mathbf{\Theta}}_\mathrm{d} & \mathbf{0} \\ * & * & * & \mathbf{I} \end{bmatrix} > 0 \tag{25}$$

Left multiplying and right multiplying the matrix above with a positive-definite block-diagonal matrix $\mathrm{diag}(\tilde{\mathbf{\Theta}}_\mathrm{d}^{-1}, \mathbf{I}, \tilde{\mathbf{\Theta}}_\mathrm{d}^{-1}, \mathbf{I})$, and letting $\mathbf{\Theta}_\mathrm{d}=\tilde{\mathbf{\Theta}}_\mathrm{d}^{-1}$, the following matrix inequality is obtained:

$$\begin{bmatrix} \mathbf{\Theta}_\mathrm{d} & \mathbf{0} & \mathbf{\Theta}_\mathrm{d}\mathbf{A}_\mathrm{dCL}^\mathrm{T} & \mathbf{\Theta}_\mathrm{d}\mathbf{C}_\mathrm{dCL}^\mathrm{T} \\ * & \gamma^2\mathbf{I} & \mathbf{E}_\mathrm{d}^\mathrm{T} & \mathbf{0} \\ * & * & \mathbf{\Theta}_\mathrm{d} & \mathbf{0} \\ * & * & * & \mathbf{I} \end{bmatrix} > 0 \tag{26}$$



DOI: 10.1002/eqe

Similar to the continuous-time system, by replacing the closed-loop matrices $\mathbf{A}_{\mathrm{dCL}}$ and $\mathbf{C}_{\mathrm{dCL}}$ in Equation (26) with their definitions in Equation (23), and letting $\mathbf{Y}_{\mathrm{d}} = \mathbf{G}_{\mathrm{d}}\boldsymbol{\Theta}_{\mathrm{d}}$, the above matrix inequality can be converted into:

$$\begin{bmatrix} \boldsymbol{\Theta}_{\mathrm{d}} & \mathbf{0} & \boldsymbol{\Theta}_{\mathrm{d}}\mathbf{A}_{\mathrm{d}}^{\mathrm{T}} + \mathbf{Y}_{\mathrm{d}}^{\mathrm{T}}\mathbf{B}_{\mathrm{d}}^{\mathrm{T}} & \boldsymbol{\Theta}_{\mathrm{d}}\mathbf{C}_{\mathbf{z}}^{\mathrm{T}} + \mathbf{Y}_{\mathrm{d}}^{\mathrm{T}}\mathbf{D}_{\mathbf{z}}^{\mathrm{T}} \\ * & \gamma^2\mathbf{I} & \mathbf{E}_{\mathrm{d}}^{\mathrm{T}} & \mathbf{0} \\ * & * & \boldsymbol{\Theta}_{\mathrm{d}} & \mathbf{0} \\ * & * & * & \mathbf{I} \end{bmatrix} > 0 \tag{27}$$

Therefore, the discrete-time $\mathscr{H}_\infty$ control problem can be converted to a convex optimization problem with LMI constraints:

$$\begin{aligned} &\text{minimize} \quad \gamma \\ &\text{subject to} \quad \boldsymbol{\Theta}_{\mathrm{d}} > 0 \text{ and the LMI expressed in Equation (27)} \end{aligned} \tag{28}$$

Here again, $\mathbf{Y}_{\mathrm{d}}$, $\boldsymbol{\Theta}_{\mathrm{d}}$, and $\gamma$ are the optimization variables. After the optimization problem is solved, the control gain matrix is computed as:

$$\mathbf{G}_{\mathrm{d}} = \mathbf{Y}_{\mathrm{d}}\boldsymbol{\Theta}_{\mathrm{d}}^{-1} \tag{29}$$

Furthermore, the sparsity pattern of the gain matrix can be obtained by specifying appropriate zero entries to the LMI variables $\mathbf{Y}_{\mathrm{d}}$ and $\boldsymbol{\Theta}_{\mathrm{d}}$, following the same procedure as described in the continuous-time case.

## 3. NUMERICAL SIMULATIONS

Since the discrete-time formulation is suitable for implementation in modern digital controllers, numerical simulations are conducted to evaluate the performance of the discrete time decentralized $\mathscr{H}_\infty$ control schemes described in Section 2.2. In Section 3.1, the procedure for designing the decentralized $\mathscr{H}_\infty$ controller is illustrated in details using a 3-story structure. Performance of the $\mathscr{H}_\infty$ controllers is compared with the performance of controllers based on the LQR optimization criteria. In Section 3.2, simulations using a 20-story benchmark structure are conducted to illustrate the efficacy of the decentralized $\mathscr{H}_\infty$ control solution for large-scale civil structures. Results using both ideal actuators and large-capacity SHD dampers are presented for the 20-story structure.

### *3.1. Numerical simulation of a 3-story structure*

*3.1.1. Decentralized $\mathscr{H}_\infty$ control.* Simulations of a 3-story shear–frame structure are first presented to illustrate the procedure employed in decentralized $\mathscr{H}_\infty$ control design. The frame structure is modeled as an in-plane lumped-mass shear structure with one actuator allocated between every two neighboring floors. It is assumed that both the inter-story drifts and inter-story velocities between every two neighboring floors are measurable. Such an assumption is reasonable



DOI: 10.1002/eqe

considering that modern SHD dampers contain internal stroke sensors and load cells that measure real-time damper displacements and forces, respectively [11]. Assuming V-brace elements are used as shown in Figure 1, the displacement and force measurements can be used to estimate inter-story drifts and velocities. The following mass, stiffness, and damping matrices are adopted for the example structure:

$$\mathbf{M}=\begin{bmatrix}6 & & \\ & 6 & \\ & & 6\end{bmatrix}\times 10^3\,\mathrm{kg},\quad \mathbf{K}=\begin{bmatrix}3.4 & -1.8 & \\ -1.8 & 3.4 & -1.6\\ & -1.6 & 1.6\end{bmatrix}\times 10^6\,\mathrm{N/m}$$
$$\mathbf{C}=\begin{bmatrix}12.4 & -5.16 & \\ -5.16 & 12.4 & -4.59\\ & -4.59 & 7.20\end{bmatrix}\times 10^3\,\mathrm{N/(m/s)} \tag{30}$$

For unidirectional ground excitation, the continuous-time system matrices **A**, **B**, and **E** can be obtained via Equation (7) as

$$\mathbf{A}=\begin{bmatrix}0 & 1 & 0 & 0 & 0 & 0\\ -266.7 & -1.2 & 300 & 0.8603 & 0 & 0\\ 0 & 0 & 0 & 1 & 0 & 0\\ 266.7 & 0.7647 & -600 & -2.156 & 266.7 & 0.7647\\ 0 & 0 & 0 & 0 & 0 & 1\\ 0 & 0 & 300 & 0.8603 & -533.3 & -1.965\end{bmatrix}$$
$$\mathbf{B}=\begin{bmatrix}0 & 0 & 0\\ -1.667 & 1.667 & 0\\ 0 & 0 & 0\\ 1.667 & -3.333 & 1.667\\ 0 & 0 & 0\\ 0 & 1.667 & -3.333\end{bmatrix}\times 10^{-4},\quad \mathbf{E}=\begin{bmatrix}0\\ -1\\ 0\\ 0\\ 0\\ 0\end{bmatrix} \tag{31}$$

Note that the state-space vector corresponding to these matrices no longer contains displacements and velocities relative to the ground. Instead, the vector has been formulated to contain inter-story drifts and velocities that are grouped by floors as given in Equation (5). The system matrices in



DOI: 10.1002/eqe

Equation (31) can be readily converted into their discrete-time equivalents for a given sampling frequency [28]. For the results presented here, a sampling frequency of 100 Hz is employed. The output matrices $\mathbf{C_z}$ and $\mathbf{D_z}$ shown in Equation (23) are defined as

$$\mathbf{C_z}=\left[\begin{array}{cccccc} 50 & 0 & 0 & 0 & 0 & 0 \\ 0 & 0 & 50 & 0 & 0 & 0 \\ 0 & 0 & 0 & 0 & 50 & 0 \\ \hline 0 & 0 & 0 & 0 & 0 & 0 \\ 0 & 0 & 0 & 0 & 0 & 0 \\ 0 & 0 & 0 & 0 & 0 & 0 \end{array}\right], \quad \mathbf{D_z}=\left[\begin{array}{ccc} 0 & 0 & 0 \\ 0 & 0 & 0 \\ 0 & 0 & 0 \\ \hline 3.162 & 0 & 0 \\ 0 & 3.162 & 0 \\ 0 & 0 & 3.162 \end{array}\right]\times 10^{-5} \tag{32}$$

The above assignments for $\mathbf{C_z}$ and $\mathbf{D_z}$ make the 2-norm of the output vector $\mathbf{z}_\mathrm{d}[k]$ a quadratic function of the inter-story drifts and control forces:

$$\begin{aligned} \|\mathbf{z}_\mathrm{d}[k]\|_2^2 &= \|(\mathbf{C_z}+\mathbf{D_z}\mathbf{G}_\mathrm{d})\mathbf{x}_\mathrm{d}[k]\|_2^2 \\ &= \|\mathbf{C_z}\mathbf{x}_\mathrm{d}[k]+\mathbf{D_z}\mathbf{u}_\mathrm{d}[k]\|_2^2 \\ &= 2500[q_1^2[k]+(q_2[k]-q_1[k])^2+(q_3[k]-q_2[k])^2] \\ &\quad +10^{-9}(u_1^2[k]+u_2^2[k]+u_3^2[k]) \end{aligned} \tag{33}$$

The decentralized $\mathscr{H}_\infty$ controller design aims to minimize the closed-loop $\mathscr{H}_\infty$-norm, which is defined as the system norm from the excitation input to the output $\mathbf{z}_\mathrm{d}$. The relative weighting between the structural response and the control effort is reflected by the magnitude of the output matrices, $\mathbf{C_z}$ and $\mathbf{D_z}$. If higher attenuation of structural response is needed, larger magnitude should be assigned to $\mathbf{C_z}$; on the contrary, if less control effort is available, larger magnitude should be assigned to $\mathbf{D_z}$. Using the matrices defined in Equations (31) and (32), the convex optimization problem as shown in Equation (28) can be posed with different sparsity patterns imposed on the $\mathbf{Y}_\mathrm{d}$ and $\mathbf{\Theta}_\mathrm{d}$ matrices. For the two sparsity patterns I and II defined in Equations (20) and (21), the solutions to the optimization problem result in the following two decentralized control gain matrices, respectively:

$$\mathbf{G}_\mathrm{dI}=\left[\begin{array}{cccccc} -1.578 & 5.608 & & & & \\ & & -5.383 & 3.195 & & \\ & & & & -4.109 & 3.013 \end{array}\right]\times 10^5 \tag{34}$$

$$\mathbf{G}_\mathrm{dII}=\left[\begin{array}{cccccc} -4.246 & 10.12 & 10.59 & 11.86 & & \\ 4.747 & 4.141 & -7.363 & 11.77 & -0.1178 & -0.0788 \\ & & 5.106 & 6.320 & -9.763 & 4.061 \end{array}\right]\times 10^5 \tag{35}$$



DOI: 10.1002/eqe

Table I. $\mathscr{H}_2$- and $\mathscr{H}_\infty$-norms of the open-loop transfer function $\mathbf{H_{zw}}$ and the closed-loop norms using both the $\mathscr{H}_\infty$ controllers and LQR controllers.

| | | Closed-loop | | | | | |
|---|---|---|---|---|---|---|---|
| | | Fully decentralized | | Partially decentralized | | Centralized | |
| | Open-loop (Uncontrolled) | $\mathbf{G}_{\mathrm{dI}}^{\mathrm{LQR}}$ | $\mathbf{G}_{\mathrm{dI}}(\mathscr{H}_\infty)$ | $\mathbf{G}_{\mathrm{dII}}^{\mathrm{LQR}}$ | $\mathbf{G}_{\mathrm{dII}}(\mathscr{H}_\infty)$ | $\mathbf{G}_{\mathrm{dIII}}^{\mathrm{LQR}}$ | $\mathbf{G}_{\mathrm{dIII}}(\mathscr{H}_\infty)$ |
| $\mathscr{H}_\infty$-norm | 8.4366 | 1.2836 | 0.8521 | 1.0462 | 0.7076 | 0.9922 | 0.7045 |
| $\mathscr{H}_2$-norm | 0.4657 | 0.1874 | 0.3020 | 0.1786 | 0.5027 | 0.1772 | 0.6108 |

When no sparsity pattern is applied to $\mathbf{Y}_\mathrm{d}$ and $\mathbf{\Theta}_\mathrm{d}$, a full gain matrix representing centralized feedback is generated

$$\mathbf{G}_{\mathrm{dIII}} = \begin{bmatrix} 2.354 & 15.24 & -0.6553 & 11.52 & 1.505 & 6.281 \\ -3.719 & 10.04 & 3.358 & 8.539 & 1.125 & 4.499 \\ -3.954 & 5.742 & -1.599 & 4.726 & 5.687 & 3.269 \end{bmatrix} \times 10^5 \tag{36}$$

The open-loop $\mathscr{H}_\infty$-norm of the uncontrolled structure and the closed-loop $\mathscr{H}_\infty$-norms of the controlled structure using the above gain matrices are listed in Table I. The $\mathscr{H}_\infty$-norm of the uncontrolled structure is computed using the discrete-time system defined in Equation (22) with the gain matrix $\mathbf{G}_\mathrm{d}$ set as a zero matrix. Comparing the four cases in Table I, the uncontrolled structure has the highest $\mathscr{H}_\infty$-norm (8.4366), which indicates the largest 'worst-case' amplification from the excitation input $\mathbf{w}_\mathrm{d}$ to the output $\mathbf{z}_\mathrm{d}$. Among the three controlled cases, because the centralized case with gain matrix $\mathbf{G}_{\mathrm{dIII}}$ assumes that complete state information is available for control decisions, the lowest $\mathscr{H}_\infty$-norm (0.7045) is achieved (which means best control performance). The fully decentralized case with gain matrix $\mathbf{G}_{\mathrm{dI}}$ has the largest norm (0.8521) among the three $\mathscr{H}_\infty$ controllers; this is somewhat expected because the fully decentralized controller has the least amount of information available for calculating control decisions for each control device.

The 1940 El Centro NS (Imperial Valley Irrigation District Station) earthquake record with its peak acceleration scaled to $1\,\mathrm{m/s^2}$ is used as the ground excitation. Three ideal actuators that generate any desired control force are deployed at the three stories. In contrast to a realistic semi-active or active control device, an ideal actuator offers unlimited force capacity, and has zero time delay while delivering the force. Maximum inter-story drifts and control forces during the dynamic response are plotted in Figure 2. The inter-story drift plots in Figure 2(a) include the results for the uncontrolled structure and the structure controlled using the three different gain matrices. Using ideal actuators, all three controlled cases achieve significant reduction in inter-story drifts compared with the uncontrolled case. Among the three controlled cases, the fully decentralized case using gain matrix $\mathbf{G}_{\mathrm{dI}}$ achieves the smallest reduction in inter-story drifts, which is consistent with the performance comparison indicated by the $\mathscr{H}_\infty$-norms in Table I. The difference between the cases using gain matrices $\mathbf{G}_{\mathrm{dII}}$ and $\mathbf{G}_{\mathrm{dIII}}$ is minor, with $\mathbf{G}_{\mathrm{dIII}}$ achieving slightly better performance.

Figure 2(b) presents the peak control forces for the three controlled cases. The fully decentralized controller imposes the lowest requirements on the control force capacity. The peak control forces are similar between the partially decentralized case $\mathbf{G}_{\mathrm{dII}}$ and the centralized case $\mathbf{G}_{\mathrm{dIII}}$. The largest sum of the three peak actuator forces is about 35 kN, which represents the total capacity of all the



DOI: 10.1002/eqe

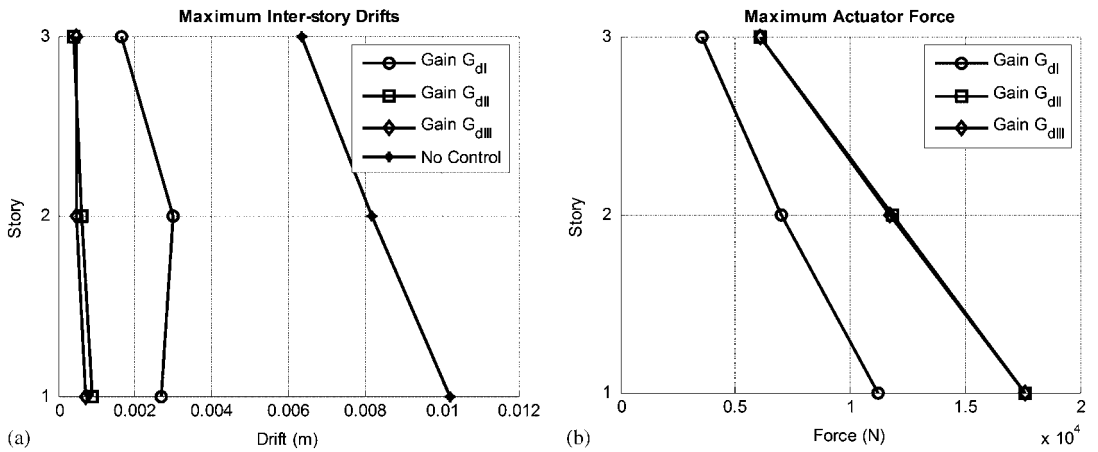


Figure 2. Simulation results when ideal actuators are deployed on the 3-story structure.

Table II. RMS values of control forces and the changes in RMS inter-story drifts ($\mathscr{H}_\infty$ control cases).

| | RMS of uncontrolled inter-story drift (mm) | Controlled | | | | | |
|---|---|---|---|---|---|---|---|
| | | $\mathbf{G}_{dI}$ | | $\mathbf{G}_{dII}$ | | $\mathbf{G}_{dIII}$ | |
| | | Drift change (%) | Force (kN) | Drift change (%) | Force (kN) | Drift change (%) | Force (kN) |
| Story-1 | 2.9 | −85 | 2.06 | −95 | 3.08 | −96 | 3.09 |
| Story-2 | 2.1 | −78 | 1.35 | −95 | 2.08 | −96 | 2.06 |
| Story-3 | 1.4 | −82 | 0.69 | −95 | 1.05 | −94 | 1.09 |
| Average | N/A | −82 | 1.37 | −95 | 2.07 | −95 | 2.08 |

actuators. This amount of total actuator capacity is about 19% of the building weight (180 kN), a realistic ratio as suggested by most references [30–32].

Further illustration of the trade-off between structural response attenuation and control effort is shown in Table II. The table first lists the root-of-mean-square (RMS) values of the inter-story drifts at all three floors when the structure is uncontrolled, i.e. 2.9, 2.1, and 1.4 mm, respectively. For the three controlled cases, changes in RMS drifts are listed in percentages relative to the uncontrolled values, i.e. negative numbers represent reduction from the uncontrolled value. For example, case $\mathbf{G}_{dIII}$ offers 96% reduction to the RMS drift at the first story. RMS values of three actuator forces are also listed for the three controlled cases. For each controlled case, the bottom row of Table II provides average drift changes and RMS forces across the three stories. It is again shown that cases $\mathbf{G}_{dII}$ and $\mathbf{G}_{dIII}$ offer greater reduction to structural response through larger control effort.

*3.1.2. Comparison with decentralized LQR control.* It could be instructive to compare the decentralized $\mathscr{H}_\infty$ controller design with the decentralized LQR controller design that was previously studied [12]. The LQR control algorithm aims to select the optimal control force trajectory $\mathbf{u}_d$ by



DOI: 10.1002/eqe

minimizing the expected value of a quadratic cost function, $J$:

$$J = \sum_{k=1}^{\infty} (\mathbf{x}_{\mathrm{d}}^{\mathrm{T}}[k]\mathbf{Q}\mathbf{x}_{\mathrm{d}}[k] + \mathbf{u}_{\mathrm{d}}^{\mathrm{T}}[k]\mathbf{R}\mathbf{u}_{\mathrm{d}}[k]), \quad \mathbf{Q}_{2n\times 2n} \geqslant 0 \quad \text{and} \quad \mathbf{R}_{m_2\times m_2} > 0 \tag{37}$$

Using the same definition of the output matrices as described in Equation (32), the following weighting matrices are employed for the LQR controller design:

$$\mathbf{Q} = \mathbf{C}_{\mathbf{z}}^{\mathrm{T}}\mathbf{C}_{\mathbf{z}} \tag{38}$$

$$\mathbf{R} = \mathbf{D}_{\mathbf{z}}^{\mathrm{T}}\mathbf{D}_{\mathbf{z}} \tag{39}$$

As a result, the LQR optimization index $J$ is proportional to the signal 2-norm of the system output:

$$\begin{aligned} J &= \sum_{k=1}^{K} (\mathbf{x}_{\mathrm{d}}^{\mathrm{T}}[k]\mathbf{C}_{\mathbf{z}}^{\mathrm{T}}\mathbf{C}_{\mathbf{z}}\mathbf{x}_{\mathrm{d}}[k] + \mathbf{u}_{\mathrm{d}}^{\mathrm{T}}[k]\mathbf{D}_{\mathbf{z}}^{\mathrm{T}}\mathbf{D}_{\mathbf{z}}\mathbf{u}_{\mathrm{d}}[k]) \\ &= \sum_{k=1}^{K} \|\mathbf{C}_{\mathbf{z}}\mathbf{x}_{\mathrm{d}}[k] + \mathbf{D}_{\mathbf{z}}\mathbf{u}_{\mathrm{d}}[k]\|_2^2 \\ &= \sum_{k=1}^{K} \|\mathbf{z}_{\mathrm{d}}[k]\|_2^2 \\ &= \|\mathbf{z}_{\mathrm{d}}\|_2^2/\Delta t \end{aligned} \tag{40}$$

where $\Delta t$ is the sampling period, and note that $\mathbf{C}_{\mathbf{z}}^{\mathrm{T}}\mathbf{D}_{\mathbf{z}} = \mathbf{0}$ and $\mathbf{D}_{\mathbf{z}}^{\mathrm{T}}\mathbf{C}_{\mathbf{z}} = \mathbf{0}$ using the definitions in Equation (32). The design of the LQR controller iteratively searches for an optimal control gain matrix by traversing along the optimization gradient. Sparsity shape constraints are iteratively applied to the search gradient in order to compute the decentralized gain matrices. The following three decentralized/centralized LQR gain matrices are obtained:

$$\mathbf{G}_{\mathrm{dI}}^{\mathrm{LQR}} = \begin{bmatrix} 4.4137 & 1.2649 & & & & \\ & & 4.6383 & 0.9489 & & \\ & & & & 5.1068 & 0.6965 \end{bmatrix} \times 10^5 \tag{41}$$

$$\mathbf{G}_{\mathrm{dII}}^{\mathrm{LQR}} = \begin{bmatrix} 5.4594 & 1.2150 & -0.3170 & 0.4404 & & \\ 0.5689 & 0.5262 & 4.0575 & 0.8687 & 0.2693 & 0.2932 \\ & & -0.1671 & 0.2163 & 5.0089 & 0.6818 \end{bmatrix} \times 10^5 \tag{42}$$

$$\mathbf{G}_{\mathrm{dIII}}^{\mathrm{LQR}} = \begin{bmatrix} 5.2399 & 1.2321 & 0.8256 & 0.5676 & 0.1599 & 0.2438 \\ 0.5157 & 0.5230 & 4.1441 & 0.8631 & 0.4141 & 0.2975 \\ 0.1322 & 0.2427 & 0.6449 & 0.3228 & 4.5696 & 0.6714 \end{bmatrix} \times 10^5 \tag{43}$$

Table I also lists the $\mathscr{H}_2$- and $\mathscr{H}_\infty$-norms of the open-loop transfer function $\mathbf{H}_{\mathbf{zw}}$ and the closed-loop norms using both the $\mathscr{H}_\infty$ controllers and the LQR controllers. Since the LQR control



DOI: 10.1002/eqe

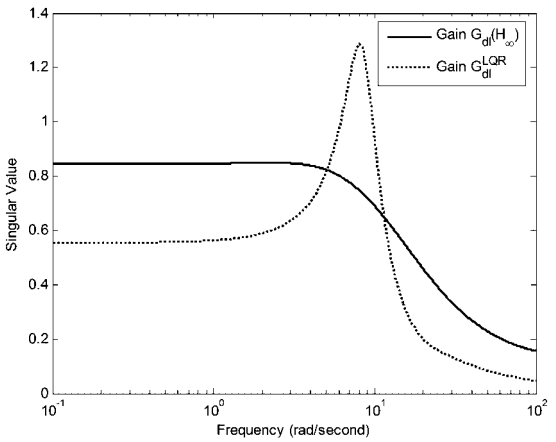


Figure 3. Singular values of the closed-loop system transfer function $\mathbf{H}_{\mathbf{zw}}(j\omega)$ using the decentralized $\mathscr{H}_\infty$ controller $\mathbf{G}_{\mathrm{dI}}$ and decentralized LQR controller $\mathbf{G}_{\mathrm{dI}}^{\mathrm{LQR}}$.

approach is equivalent to an $\mathscr{H}_2$ control design that minimizes the closed-loop $\mathscr{H}_2$-norm, LQR controllers are expected to perform well in reducing the closed-loop $\mathscr{H}_2$-norm [14, 33]. Similar to the $\mathscr{H}_\infty$-norm, definition of the system $\mathscr{H}_2$-norm can also be written in terms of the singular values of the transfer function matrix:

$$\|\mathbf{H}_{\mathbf{zw}}(s)\|_2 = \sqrt{\frac{1}{2\pi}\int_{-\infty}^{+\infty} \sum_i \sigma_i^2[\mathbf{H}_{\mathbf{zw}}(j\omega)]\,\mathrm{d}\omega} \tag{44}$$

As expected, Table I shows that the LQR controllers, no matter decentralized or centralized, consistently perform better than their $\mathscr{H}_\infty$ counterparts in reducing the $\mathscr{H}_2$-norm, while the $\mathscr{H}_\infty$ controllers consistently perform better than their LQR counterparts in terms of reducing the $\mathscr{H}_\infty$-norm.

In this example, the second dimension of the transfer function matrix $\mathbf{H}_{\mathbf{zw}}(j\omega)$ is one, because the disturbance $\mathbf{w}$ is a scalar that represents the ground excitation. Therefore, $\mathbf{H}_{\mathbf{zw}}(j\omega)$ has only one singular value at each frequency $\omega$, which is the largest singular value. Figure 3 plots the singular value of the closed-loop system transfer function $\mathbf{H}_{\mathbf{zw}}(j\omega)$ using the decentralized $\mathscr{H}_\infty$ controller $\mathbf{G}_{\mathrm{dI}}$ and the decentralized LQR controller $\mathbf{G}_{\mathrm{dI}}^{\mathrm{LQR}}$. The definition of the system $\mathscr{H}_\infty$-norm in Equation (12) shows that the $\mathscr{H}_\infty$-norm should be equal to the peak of the largest singular value over the frequency span. Correspondingly, Figure 3 shows that the peak of the singular value using the $\mathscr{H}_\infty$ controller $\mathbf{G}_{\mathrm{dI}}$ is about 0.85, while the peak for the LQR controller $\mathbf{G}_{\mathrm{dI}}^{\mathrm{LQR}}$ is about 1.28; both of which are consistent with the $\mathscr{H}_\infty$-norms listed in Table I. Figure 3 also illustrates that the decentralized $\mathscr{H}_\infty$ controller excels at 'pushing down the peak of the largest singular value.' In comparison, the decentralized LQR controller is shown to excel in reducing all singular values over the entire frequency span, which agrees with the objective of minimizing the $\mathscr{H}_2$-norm (as defined in Equation (44)).

Simulations are conducted using the LQR controllers, with the same 1940 El Centro NS earthquake excitation scaled to $1\,\mathrm{m/s^2}$. Three ideal actuators are again deployed at the three stories. Maximum inter-story drifts and control forces during the dynamic response are plotted in Figure 4.



DOI: 10.1002/eqe

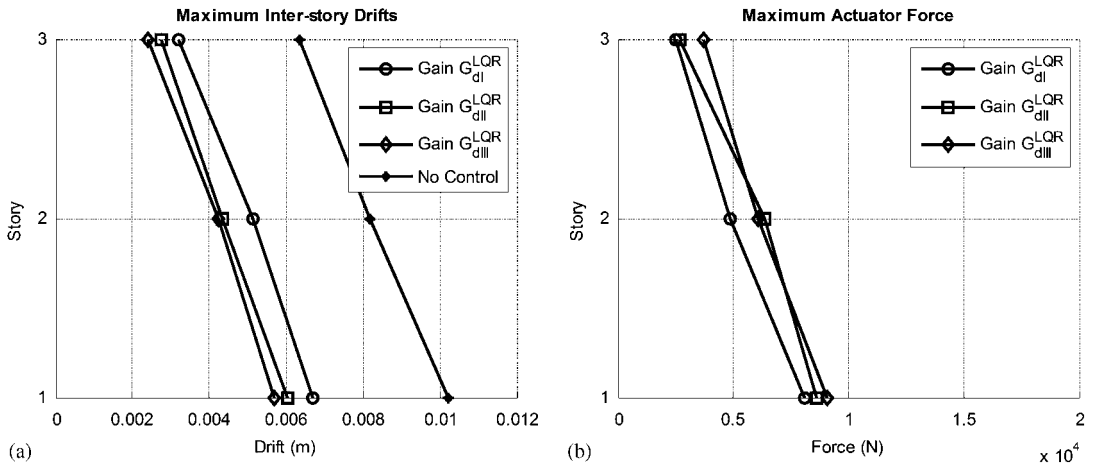


Figure 4. Simulation results when ideal actuators are deployed on the 3-story structure.

Comparison between Figures 2 and 4 show that LQR controllers generally achieve less reduction to peak inter-story drifts. On the other hand, the advantage of the LQR controllers in this example is that they impose lower requirements to the force capacity of the structural control devices. For the LQR control cases, the total actuator capacity is approximately 20 kN, i.e. about 11% of the building weight. This ratio is much lower than the ratio of 19% for the $\mathscr{H}_\infty$ control cases.

Similar to Table II for the $\mathscr{H}_\infty$ control cases, further illustration of the trade-off between structural response attenuation and control effort is shown in Table III for LQR control. For the controlled cases, changes in RMS drifts are again listed in percentages relative to the uncontrolled values. The table shows that as compared with case $\mathbf{G}_{\mathrm{dI}}^{\mathrm{LQR}}$, cases $\mathbf{G}_{\mathrm{dII}}^{\mathrm{LQR}}$ and $\mathbf{G}_{\mathrm{dIII}}^{\mathrm{LQR}}$ offer greater reduction to structural response at the expense of larger control effort. Comparing the bottom rows of Tables II and III, it is again illustrated that the LQR cases achieve less attenuation to structural response, while demanding less control effort.

### *3.2. Numerical simulation of a 20-story benchmark structure*

*3.2.1. Simulation using ideal actuators.* To explore the performance of decentralized $\mathscr{H}_\infty$ control for a larger-scale structure, a 20-story benchmark building designed for the Structural Engineers Association of California (SAC) project is selected [34]. Same as the 3-story example, discrete-time controllers are adopted in the simulation. The building is modeled as an in-plane lumped-mass shear structure with control devices allocated between every set of neighboring floors. Figure 5(a) shows the mass, stiffness, and damping parameters of the structure. In the numerical simulations, it is assumed that both the inter-story drifts and inter-story velocities between every two neighboring floors are measurable. As shown in Equation (5), the state-space equations are formulated such that the state-space vector contains inter-story drifts and velocities. Simulations are conducted for different decentralization schemes as shown in Figure 5(b). The degree-of-centralization (DC) reflects the different communication architectures, with each communication subnet (as denoted by channels Ch1, Ch2, etc.) covering a limited number of stories. The controllers covered by a subnet are allowed to access the sensor data within that subnet. For example, the case where DC = 1 has each subnet covering only five stories with a total of four subnets utilized. For DC = 2, each



DOI: 10.1002/eqe

Table III. RMS values of control forces and the changes in RMS inter-story drifts (LQR control cases).

| | RMS of uncontrolled inter-story drift (mm) | Controlled | | | | | |
|---|---|---|---|---|---|---|---|
| | | $\mathbf{G}_{\mathrm{dI}}^{\mathrm{LQR}}$ | | $\mathbf{G}_{\mathrm{dII}}^{\mathrm{LQR}}$ | | $\mathbf{G}_{\mathrm{dIII}}^{\mathrm{LQR}}$ | |
| | | Drift change (%) | Force (kN) | Drift change (%) | Force (kN) | Drift change (%) | Force (kN) |
| Story-1 | 2.9 | −66 | 1.20 | −71 | 1.32 | −73 | 1.42 |
| Story-2 | 2.1 | −65 | 0.76 | −71 | 1.04 | −72 | 1.01 |
| Story-3 | 1.4 | −67 | 0.42 | −72 | 0.46 | −75 | 0.59 |
| Average | N/A | −66 | 0.79 | −71 | 0.94 | −73 | 1.01 |

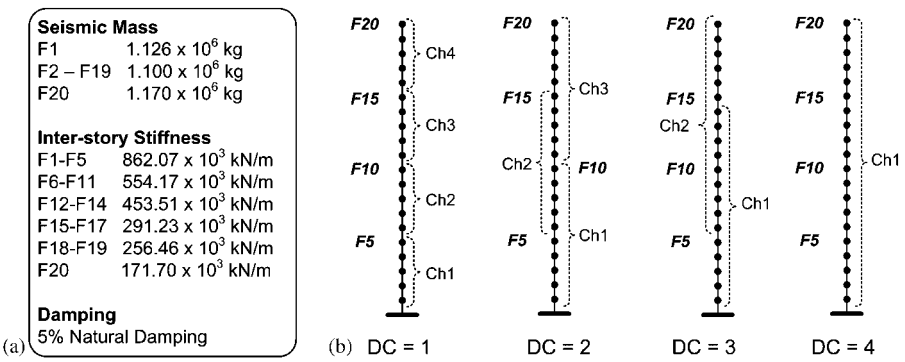


Figure 5. Twenty-story SAC building for numerical simulations: (a) model parameters of the lumped-mass structure and (b) communication subnet partitioning for different degrees-of-centralization (DC).

subnet covers 10 stories and a total of three subnets are utilized; meanwhile, overlaps exist between subnets for DC = 2. For stories covered by multiple overlapping subnets, each controller at these stories should have communication access to data within all the overlapping subnets. Although each controller may command multiple control devices, in this example, a control device can only be commanded by one controller. The gain matrices for the decentralized information structures with DC = 1 and 2 have the following sparsity patterns:

$$\mathbf{G}_{\mathbf{d}} = \begin{bmatrix} \blacksquare & & & \\ \blacksquare & \blacksquare & & \\ & \blacksquare & \blacksquare & \\ & & \blacksquare & \blacksquare \end{bmatrix}_{20\times 40} \text{when DC} = 1; \quad \mathbf{G}_{\mathbf{d}} = \begin{bmatrix} \blacksquare & \blacksquare & & \\ \blacksquare & \blacksquare & \blacksquare & \\ & \blacksquare & \blacksquare & \blacksquare \\ & & \blacksquare & \blacksquare \end{bmatrix}_{20\times 40} \text{when DC} = 2 \tag{45}$$

Each entry in the above matrices represents a $5\times$ 10 block submatrix. To achieve the sparsity patterns in gain matrix $\mathbf{G}_{\mathrm{d}}$, the matrix variable $\mathbf{Y}_{\mathrm{d}}$ in Equation (28) is defined to have the same sparsity pattern as $\mathbf{G}_{\mathrm{d}}$, and $\mathbf{\Theta}_{\mathrm{d}}$ is defined to be always block-diagonal. For the cases where DC = 3 and 4, the number of stories covered by each communication subnet increases accordingly, which result in fewer zero blocks in $\mathbf{G}_{\mathrm{d}}$. Clearly, the case where DC = 4 corresponds to a centralized feedback structure with all devices in the same subnet (i.e. Ch1).



DOI: 10.1002/eqe

To investigate the effectiveness of the proposed decentralized control design, we first assume the 20-story structure is instrumented with ideal actuators that can produce any desired force. Output matrices $\mathbf{C_z}$ and $\mathbf{D_z}$ in Equation (23) are defined as

$$\mathbf{C_z} = \begin{bmatrix} 10^2\mathbf{I}_{40\times 40} \\ \mathbf{0}_{20\times 40} \end{bmatrix}, \quad \mathbf{D_z} = \begin{bmatrix} \mathbf{0}_{40\times 20} \\ 10^{-12}\mathbf{I}_{20\times 20} \end{bmatrix} \tag{46}$$

Simulations are performed for different DCs (DC$=1,\ldots,4$) and sampling periods (ranging from 0.01 to 0.06 s at a resolution of 0.01 s). Additionally, three ground motion records all scaled to a peak ground acceleration (PGA) of $1\,\mathrm{m/s^2}$ are used for the simulation: 1940 El Centro NS (Imperial Valley Irrigation District Station), 1995 Kobe NS (JMA Station), and 1999 Chi-Chi NS (TCU-076 Station). Two representative performance indices, $J_1$ and $J_2$, as proposed by Spencer *et al*. [34] are adopted:

$$J_1 = \max_{\text{Earthquakes}} \left\{ \max_{k,i} d_i[k] \Big/ \max_{k,i} \hat{d}_i[k] \right\} \tag{47}$$

$$J_2 = \max_{\text{Earthquakes}} \{\|\mathbf{z}_\mathrm{d}\|_2^2 / \|\hat{\mathbf{z}}_\mathrm{d}\|_2^2\} \tag{48}$$

Here $J_1$ and $J_2$ correspond to maximum inter-story drifts and output vector $\mathbf{z}_\mathrm{d}$, respectively. In Equation (47), $d_i[k]$ represents the inter-story drift between floor $i$ ($i=1,\ldots,n$) and its lower floor at time step $k$, and $\max_{k,i} d_i[k]$ is the maximum inter-story drift over the entire time history and among all floors. The maximum inter-story drift is normalized by its counterpart $\max_{k,i} \hat{d}_i[k]$, which is the maximum response of the uncontrolled structure. The largest normalized ratio among the simulations for the three different earthquake records is defined as the performance index $J_1$. Similarly, the performance index $J_2$ is defined in Equation (48) based on the 2-norm of the output vector $\mathbf{z}_\mathrm{d}$; i.e. $\|\mathbf{z}_\mathrm{d}\|_2^2 = \Delta t \sum_{k=1}^{K} \mathbf{z}_\mathrm{d}^\mathrm{T}[k]\mathbf{z}_\mathrm{d}[k]$, with $K$ being the last time step of the simulation. When computing the two indices, a uniform sampling period of 0.001 s is used to collect the structural response data points for $d_i[k]$ and $\mathbf{z}_\mathrm{d}[k]$, regardless of the sampling period of the feedback control scheme. Because these indices have been normalized against the performance of the uncontrolled structure, values less than 1 indicate that the closed-loop control solution is effective with smaller index values indicating better overall control performance.

Figure 6 shows the control performance indices for DCs and sampling rates. Generally speaking, control performance is better for higher DCs and shorter sampling periods. The plots show that all control schemes achieve obvious reduction in structural response when compared with the uncontrolled case, i.e. the normalized performance indices are much less than 1. To better review the simulation results, the performance indices for the four different control schemes are re-plotted as a function of sampling period in Figure 6(c) and (d). Figure 6(d) clearly illustrates the expected comparison among the four control cases, i.e. for each sampling time, the achieved output norm generally decreases as the DC increases.

While it may appear from Figure 6 that a centralized control architecture always performs better than decentralized ones operating at the same sampling frequency, such a centralized system with high nodal counts might be economically and technically difficult to implement in large-scale civil structures. For example, significant communication and computation resources are usually required to implement a large-scale centralized control system. As a result, longer sampling periods need to be adopted which, in turn, reduces the effectiveness of the centralized solution. In contrast, if a decentralized architecture is implemented, the control system would be capable of shorter sampling



DOI: 10.1002/eqe

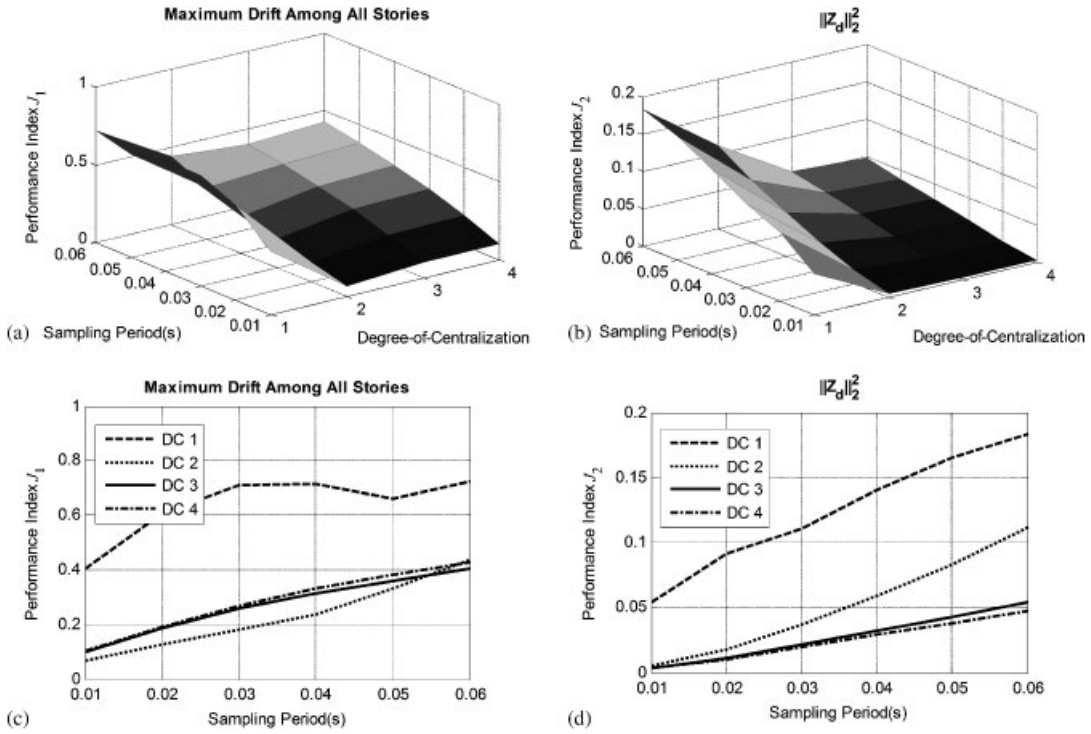


Figure 6. Simulation results for the 20-story SAC building instrumented with ideal actuators. The plots illustrate performance indices for different sampling steps and degrees-of-centralization (DC): (a) 3D plot for performance index $J_1$; (b) 3D plot for performance index $J_2$; (c) condensed 2D plot for $J_1$; and (d) condensed 2D plot for $J_2$.

periods that lead to potential improvement in the control performance. It can be observed from Figure 6 that if shorter sampling periods are adopted in partially decentralized control systems (DC2 or DC3), smaller performance indices can be achieved when compared with a centralized system (DC4) that adopts a longer sampling period. The trade-off between centralization and sampling period will be further explored in the next simulation analysis.

*3.2.2. Simulation using SHD dampers.* To investigate the performance of decentralized $\mathscr{H}_\infty$ control using realistic structural control devices, SHD dampers are employed in the simulations for the 20-story structure. The arrangement of SHD dampers in the building is shown in Figure 7(a). From lower to higher floors, the number of instrumented SHD dampers decreases gradually from 4 to 1. Figure 7(b) shows the installation of a SHD damper between two floors using a V-brace, together with key parameters of the damper. To accurately model the damping force, the Maxwell element proposed by Hatada *et al.* [35] is employed. In a Maxwell element, a dashpot and a stiffness spring are connected in series, which result in a damping force described by the following differential equation:

$$\dot{u}(t)+\frac{k_{\text{eff}}}{c_{\text{SHD}}(t)}u(t)=k_{\text{eff}}\Delta\dot{q}(t) \tag{49}$$



DOI: 10.1002/eqe

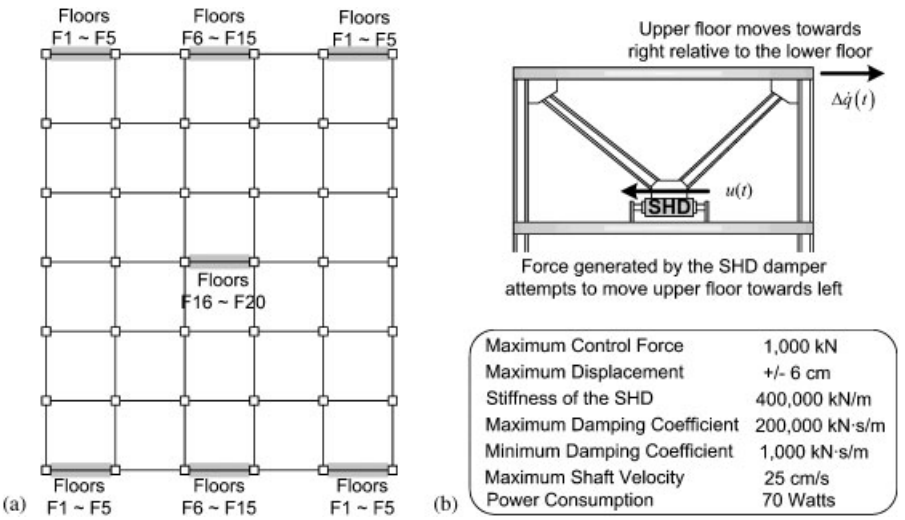


Figure 7. Instrumentation of semi-active hydraulic dampers (SHD) in the 20-story structure: (a) layout of dampers on the floor plans and (b) key parameters of the dampers.

where $u(t)$ and $\Delta\dot{q}(t)$ denote the damping force and the inter-story velocity, respectively, $k_{\text{eff}}$ represents the effective stiffness of the damper in series with the V-brace, and $c_{\text{SHD}}(t)$ is the adjustable damping coefficient of the SHD damper.

When the SHD damper is deployed in a feedback control system, if the desired damping force $u(t)$ is in an opposite direction to the inter-story velocity $\Delta\dot{q}(t)$, as shown in Figure 7(b), the damping coefficient $c_{\text{SHD}}(t)$ is adjusted so that the damper generates a force closest to the desired force. If the desired force is in the same direction to the inter-story velocity, the damping coefficient is set to its minimum value at 1000 kN s/m.

An important criterion to consider in evaluating a feedback control system, whether being centralized or decentralized, is that the feedback control system should perform better than a passive control system. When the SHD dampers are employed, fixing the damping coefficients of all dampers at either minimum (1000 kN s/m) or maximum (200 000 kN s/m) values constitutes a passive control system. Figure 8 presents the simulated maximum inter-story drifts when the structure is excited using the three ground motions with the PGA scaled to 1 m/s$^2$: 1940 El Centro NS, 1995 Kobe NS, and 1999 Chi-Chi NS. Four cases are plotted for each earthquake: the case without control, the passive case with minimum damping, the passive case with maximum damping, and a decentralized semi-active control case. For the decentralized semi-active control case, the DC is 2 (Figure 5) and the sampling frequency is 100 Hz. It is found that the decentralized $\mathscr{H}_\infty$ controller with the following output matrices, $\mathbf{C_z}$ and $\mathbf{D_z}$

$$\mathbf{C_z} = \begin{bmatrix} 10^5 \mathbf{I}_{40\times 40} \\ \mathbf{0}_{20\times 40} \end{bmatrix}, \quad \mathbf{D_z} = \begin{bmatrix} \mathbf{0}_{40\times 20} \\ 10^{-5.5} \mathbf{I}_{20\times 20} \end{bmatrix} \tag{50}$$

achieves satisfactory results. As shown in Figure 8, all three control schemes, including two passive and one semi-active, reduce the maximum inter-story drifts compared with the uncontrolled case.



DOI: 10.1002/eqe

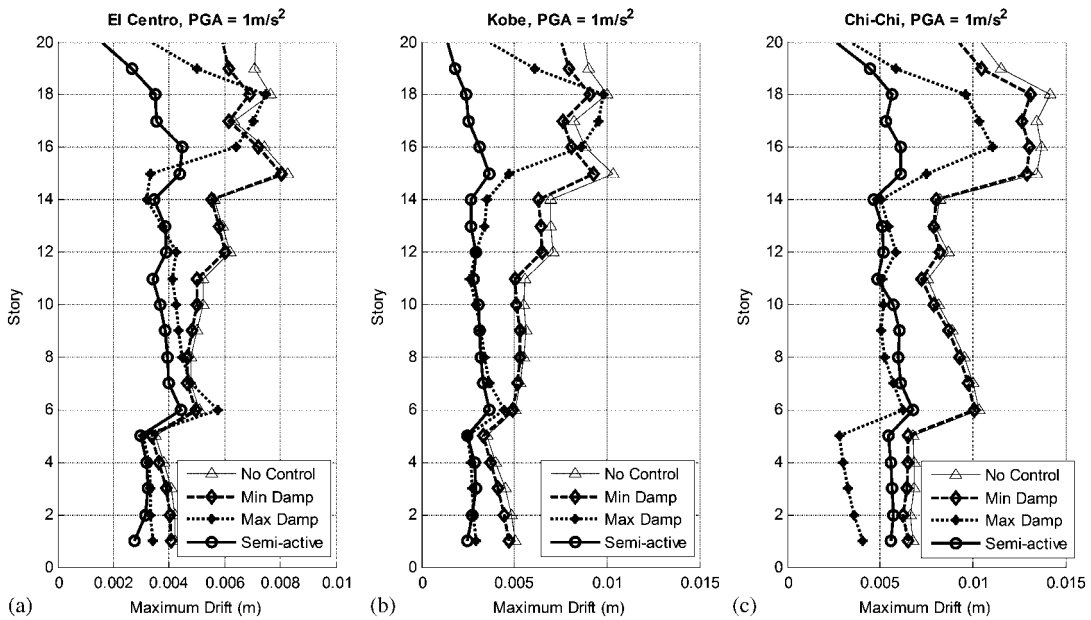


Figure 8. Maximum inter-story drifts for cases without control, with passive control (damping coefficients of all SHD dampers fixed at minimum or maximum), and with decentralized semi-active control (DC = 2 and 100 Hz sampling frequency).

The passive control case with maximum damping generally results in less inter-story drifts than the passive case with minimum damping, except at a few higher floors for the El Centro and Kobe earthquakes. The decentralized semi-active control case not only effectively reduces drifts at lower floors, but also achieves greater mitigation of drifts at the higher floors compared with the two passive cases. Better performance of the decentralized semi-active control case is observed for all three earthquake records. For the Kobe earthquake, decentralized semi-active control reduces the drift at the 18th story by about 75% compared with the uncontrolled and the two passive control cases. This shows that in the passive case with maximum damping, dampers at each story may only attempt to reduce local responses and results in conflict among damper efforts at different stories. While in the semi-active control case that aims to minimize the overall $\mathscr{H}_\infty$-norm of the global structural system, efforts from dampers at different stories can be better coordinated to reduce overall structural response.

Figure 9 compares the performance indices for the 20-story structure instrumented with SHD dampers, when different control schemes are adopted. The two passive control schemes include the maximum and minimum damping cases. To illustrate the effect of faster sampling frequency (i.e. shorter sampling periods) in decentralized feedback control, feedback control cases with different centralization degrees (DC $= 1, \ldots, 4$) are associated with different sampling frequencies. For each centralization degree, the sampling frequency is selected in reverse proportion to the number of stories contained in one communication subnet (shown in Figure 5). For example, a sampling frequency of 100 Hz is associated with case DC2, while a sampling frequency of 50 Hz is associated with the centralized case DC4 due to larger communication and computation burdens.



DOI: 10.1002/eqe

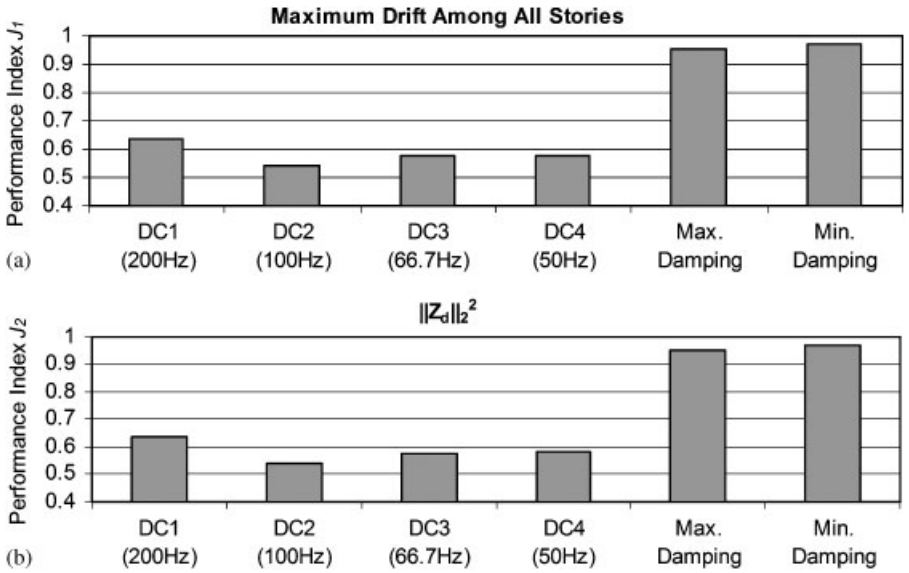


Figure 9. Simulation results for the 20-story SAC building instrumented with semi-active hydraulic dampers (SHD). The plots illustrate performance indices for passive control cases and semi-active feedback control cases with different degrees-of-centralization (DC) and sampling frequencies: (a) performance index $J_1$ and (b) performance index $J_2$.

The same three ground motion records scaled to a peak acceleration of $1\,\mathrm{m/s^2}$ are used in the simulation: 1940 El Centro NS, 1995 Kobe NS (JMA Station), and 1999 Chi-Chi. As shown in Figure 9, the feedback control cases generally achieve better performance when compared with the two passive control cases. Furthermore, the figure illustrates that although decentralized feedback control cases do not have complete sensor data available when calculating control decisions, they may outperform the centralized case due to the faster sampling frequencies that are available through decentralization. For example, compared with the centralized scheme DC4 (at 50 Hz), the partially decentralized scheme DC2 (at 100 Hz) can provide larger reduction to both maximum inter-story drift and the 2-norm of the output vector $\mathbf{z}_d$.

## 4. SUMMARY AND CONCLUSION

This paper presents pilot studies in exploring decentralized structural control design that minimizes the closed-loop $\mathscr{H}_\infty$-norm. The decentralized control design offers promising solutions to large-scale structural sensing and control systems. Solutions are developed for both continuous-time and discrete-time formulations. The properties of linear matrix inequalities are utilized to convert the complicated decentralized $\mathscr{H}_\infty$ control problem into a simple convex optimization problem. For such a convex optimization problem, decentralized architectures can be easily incorporated to yield decentralized $\mathscr{H}_\infty$ control solutions. Such solutions are necessary to provide control systems with the ability to scale with the number of sensors and actuators implemented in the system. Nevertheless, it should be noted that the shape constraining approach for decentralized



DOI: 10.1002/eqe

$\mathscr{H}_\infty$ controller design is heuristic. The approach may not guarantee the minimum $\mathscr{H}_\infty$-norm over the complete solution space.

Numerical simulation results using a 3-story and a 20-story structure illustrate the feasibility of the different decentralized control architectures. Comparison between the performance of the decentralized $\mathscr{H}_\infty$ controllers and the performance of decentralized LQR-based controllers illustrates that both controllers deliver expected performance. Using the simulation results for the 3-story structure, the trade-off between structural response attenuation and control effort is demonstrated for both the $\mathscr{H}_\infty$ controllers and LQR controllers. The ratio of the required total actuator capacity over the building weight appears realistic for both types of controllers. For the 20-story structure, the simulation results demonstrate that when realistic semi-active control devices (such as the SHD dampers) are used in combination with the decentralized $\mathscr{H}_\infty$ control algorithm, better performance can be gained over the passive control cases. It is also illustrated that decentralized control strategies may provide equivalent or even superior control performance, given that their centralized counterparts could suffer longer sampling periods due to communication and computation constraints. On the other hand, since the proposed control design is based on the assumption of system linearity, further investigation on how to improve the control performance with nonlinear semi-active control devices is needed.

The drawbacks of the presented decentralized $\mathscr{H}_\infty$ control design include the inability to consider the effect of time delay in the feedback loop and the requirement for inter-story drift and velocity data for feedback. Future research in decentralized $\mathscr{H}_\infty$ control may consider time delay effects in the control algorithm and utilize system output feedback. Furthermore, dynamic output feedback will be explored instead of static feedback, to capitalize on a much larger controller parametric space. Comparative studies will then be conducted between the decentralized $\mathscr{H}_\infty$ and decentralized LQR control designs with consideration of time-delay effects [12]. Future investigation may also include developing a systematic method for the design of decentralized architectures, e.g. the delineation of overlapping subnets, as well as the selection of appropriate degrees of centralization.

## ACKNOWLEDGEMENTS

This research is partially funded by the Office of Naval Research through the Young Investigator Award received by Prof. Jerome P. Lynch at the University of Michigan. Part of the research was accomplished during Prof. Yang Wang's PhD study at Stanford University, where he was supported by the Office of Technology Licensing Stanford Graduate Fellowship. This research is also partially supported by NSF, Grant Number CMMI-0824977 to Stanford University. The authors would like to thank Prof. Chin-Hsiung Loh of the National Taiwan University for sharing the 3-story structure model, which is based on an experimental structure built at the National Center for Research on Earthquake Engineering in Taiwan. Last but not least, the authors would like to thank the anonymous reviewers for their valuable comments and suggestions.

## REFERENCES

1. Soong TT. *Active Structural Control*: *Theory and Practice*. Wiley: Harlow, Essex, England, 1990.
2. Spencer Jr BF, Nagarajaiah S. State of the art of structural control. *Journal of Structural Engineering* 2003; **129**(7):845–856.
3. Yao JTP. Concept of structural control. *Journal of Structural Division* (ASCE) 1972; **98**(7):1567–1574.



DOI: 10.1002/eqe

4. Housner GW, Bergman LA, Caughey TK, Chassiakos AG, Claus RO, Masri SF, Skelton RE, Soong TT, Spencer Jr BF, Yao JTP. Structural control: past, present, and future. *Journal of Engineering Mechanics* 1997; **123**(9):897–971.
5. Chu SY, Soong TT, Reinhorn AM. *Active*, *Hybrid*, *Semi-active Structural Control*: *A Design*, *Implementation Handbook*. Wiley: Hoboken, NJ, 2005.
6. Soong TT, Spencer Jr BF. Supplemental energy dissipation: state-of-the-art and state-of-the-practice. *Engineering Structures* 2002; **24**(3):243–259.
7. Sandell Jr N, Varaiya P, Athans M, Safonov M. Survey of decentralized control methods for large scale systems. *IEEE Transactions on Automatic Control* 1978; **23**(2):108–128.
8. Siljak DD. *Decentralized Control of Complex Systems*. Academic Press: Boston, 1991.
9. Lunze J. *Feedback Control of Large Scale Systems*. Prentice-Hall: Englewood Cliffs, NJ, 1992.
10. Shimizu K, Yamada T, Tagami J, Kurino H. Vibration tests of actual buildings with semi-active switching oil damper. *Proceedings of the 13th World Conference on Earthquake Engineering*, Vancouver, BC, Canada, 1–6 August, 2004.
11. Kurino H, Tagami J, Shimizu K, Kobori T. Switching oil damper with built-in controller for structural control. *Journal of Structural Engineering* 2003; **129**(7):895–904.
12. Wang Y, Swartz RA, Lynch JP, Law KH, Lu K-C, Loh C-H. Decentralized civil structural control using real-time wireless sensing and embedded computing. *Smart Structures and Systems* 2007; **3**(3):321–340.
13. Wang Y. Wireless sensing and decentralized control for civil structures: theory and implementation. *Ph.D. Thesis*, Department of Civil and Environmental Engineering, Stanford University, Stanford, CA, 2007.
14. Skogestad S, Postlethwaite I. *Multivariable Feedback Control*: *Analysis and Design*. Wiley: Chichester, West Sussex, England, 2005.
15. Balandin DV, Kogan MM. LMI-based optimal attenuation of multi-storey building oscillations under seismic excitations. *Structural Control and Health Monitoring* 2005; **12**(2):213–224.
16. Chase JG, Smith HA. Robust $H_\infty$ control considering actuator saturation. I: theory. *Journal of Engineering Mechanics* 1996; **122**(10):976–983.
17. Jabbari F, Schmitendorf WE, Yang JN. $H_\infty$ control for seismic-excited buildings with acceleration feedback. *Journal of Engineering Mechanics* 1995; **121**(9):994–1002.
18. Lin C-C, Chang C-C, Chen H-L. Optimal $H_\infty$ output feedback control systems with time delay. *Journal of Engineering Mechanics* 2006; **132**(10):1096–1105.
19. Mahmoud MS, Terro MJ, Abdel-Rohman M. An LMI approach to $H_\infty$-control of time-delay systems for the benchmark problem. *Earthquake Engineering and Structural Dynamics* 1998; **27**(9):957–976.
20. Johnson EA, Voulgaris PG, Bergman LA. Multiobjective optimal structural control of the Notre Dame building model benchmark. *Earthquake Engineering and Structural Dynamics* 1998; **27**(11):1165–1187.
21. Narasimhan S, Nagarajaiah S. Smart base isolated buildings with variable friction systems: $H_\infty$ controller and SAIVF device. *Earthquake Engineering and Structural Dynamics* 2006; **35**(8):921–942.
22. Yang JN, Lin S, Jabbari F. $H_\infty$-based control strategies for civil engineering structures. *Structural Control and Health Monitoring* 2004; **11**(3):223–237.
23. Wang S-G. Robust active control for uncertain structural systems with acceleration sensors. *Journal of Structural Control* 2003; **10**(1):59–76.
24. Chase JG, Smith HA, Suzuki T. Robust $H_\infty$ control considering actuator saturation. II: applications. *Journal of Engineering Mechanics* 1996; **122**(10):984–993.
25. Boyd S, El Ghaoui L, Feron E, Balakrishnan V. *Linear Matrix Inequalities in System and Control Theory*. SIAM: Philadelphia, PA, 1994.
26. Zhou K, Doyle JC, Glover K. *Robust and Optimal Control*. Prentice-Hall: Englewood Cliffs, NJ, 1996.
27. Gahinet P. *LMI Control Toolbox for Use with MATLAB*. MathWorks Inc.: Natick, MA, 1995.
28. Grant M, Boyd S. CVX: Matlab software for disciplined convex programming (web page and software). http://stanford.edu/~boyd/cvx (18 June 2008).
29. Franklin GF, Powell JD, Workman ML. *Digital Control of Dynamic Systems*. Addison-Wesley: Menlo Park, CA, 1998.
30. Kim J-H, Jabbari F. Actuator saturation and control design for buildings under seismic excitation. *Journal of Engineering Mechanics* 2002; **128**(4):403–412.
31. Barroso LR, Chase JG, Hunt S. Resettable smart dampers for multi-level seismic hazard mitigation of steel moment frames. *Journal of Structural Control* 2003; **10**(1):41–58.
32. Kannan S, Uras HM, Aktan HM. Active control of building seismic response by energy dissipation. *Earthquake Engineering and Structural Dynamics* 1995; **24**(5):747–759.



DOI: 10.1002/eqe

33. Burl JB. *Linear Optimal Control*: $H_2$ *and* $H_\infty$ *Methods*. Addison-Wesley Longman: Menlo Park, CA, 1999.
34. Spencer Jr BF, Christenson RE, Dyke SJ. Next generation benchmark control problem for seismically excited buildings. *Proceedings of the 2nd World Conference on Structural Control*, Kyoto, Japan, 29 June–2 July 1998.
35. Hatada T, Kobori T, Ishida M, Niwa N. Dynamic analysis of structures with Maxwell model. *Earthquake Engineering and Structural Dynamics* 2000; **29**(2):159–176.



DOI: 10.1002/eqe